Supporting Information

Mechanism exploration of ion transport in nanocomposite cation exchange membranes

Xin Tong[1], Bopeng Zhang[1], Yilin Fan, and Yongsheng Chen[*]

School of Civil and Environmental Engineering, Georgia Institute of Technology,

Atlanta, GA 30332, United States

*Corresponding authors. *Tel.: +1 404 894 3089.*

E-mail address: yongsheng.chen@ce.gatech.edu *(Y. Chen).*

1 The first and second authors contributed equally to this work.

S1. Chemical Reaction of Sulfonation of Silica NPs

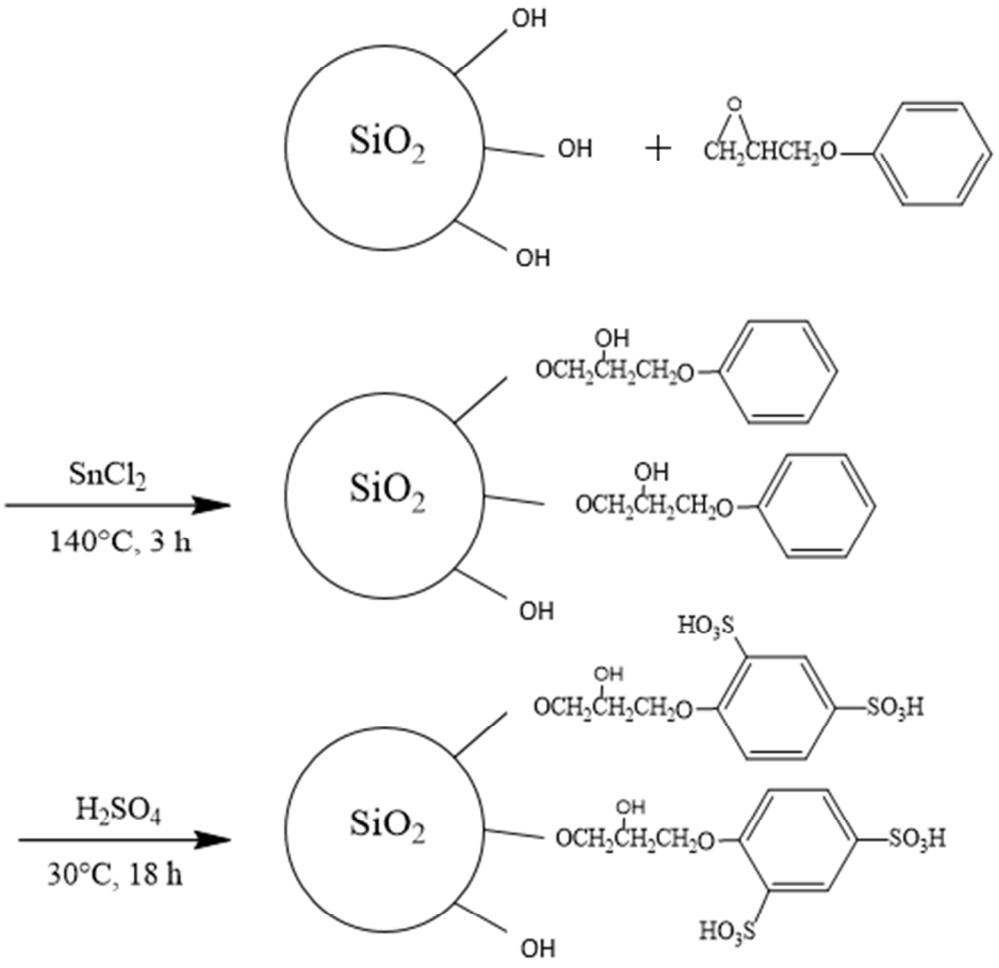

Figure S1. Scheme of sulfonation reaction of silica NPs

S2. Molecular Weight of Sulfonated and Unsulfonated Silica NPs

Hydroxyl groups are attached onto the surface of silica NPs. For the calculation of molar weight of sulfonated silica NPs, first by assuming that all the hydroxyl groups are reacted, then

$$M_{silica\ NPs,sulfonated} = \frac{M_{silica} + M_{functional\ groups}}{1\ mol} \quad \text{(S1)}$$

$$= \frac{60\text{g} + \left(\frac{0.82 \times 10^{-3}}{2} \times 325\right)\text{g}}{1\ \text{mol}}$$

$$= \frac{60\text{g} + 0.13\text{g}}{1\text{mol}}$$

$$\approx 60\text{g/mol}$$

Before the sulfonation reaction, all the functional groups were hydroxyl groups that attached on the NP surfaces.

$$M_{silica\ NPs,unfunctionalized} = \frac{M_{silica} + M_{hydroxyl\ groups}}{1\ mol} \quad \text{(S2)}$$

$$= \frac{60\text{g} + \left(\frac{0.82 \times 10^{-3}}{2} \times 17\right)\text{g}}{1\ \text{mol}}$$

$$\approx 60\text{g/mol}$$

So the molecular weight of silica NPs is almost unchanged during the sulfonation reaction. Thus, different silica NPs have different weight percentage as long as they have different molar numbers.

S3. Characterization of IEMs

The membrane sample in the acid form (H^+) was immersed into 1 M of NaCl for 6 hours. The resulting NaCl solution containing released protons was then titrated with 0.01 M of NaOH solution by using phenolphthalein as an indicator. Then the membrane sample was immersed in DI water for one day. After that, the wet membrane sample was weighted immediately after mopping with filter paper. The membrane sample was then dried in the oven at 50 °C until a constant weight (as dry weight) was obtained. The membrane IEC and swelling degree (SD) were then calculated by:

$$IEC = \frac{C_{NaOH} \times V_{NaOH}}{W_{dry}} \quad \text{(S3)}$$

$$SD = \frac{W_{wet} - W_{dry}}{W_{dry}} \times 100\% \quad \text{(S4)}$$

where C_{NaOH} is the concentration (M) of NaOH solution used, V_{NaOH} is the volume (L) of the NaOH solution, and W_{wet} and W_{dry} are the mass (g) of wet and dried membrane samples, respectively. All the measurements were conducted for at least three times.

Membrane porosity was calculated by using measured membrane weight data [1]:

$$Porosity = \frac{W_{wet} - W_{dry}}{A\delta\rho_w} \times 100\% \text{ (S5)}$$

where A is area of wet membrane sample, δ is the thickness of wet membrane sample, and ρ_w is the density of water.

Membrane apparent permselectivity was determined by calculating the ratio of measured membrane potential and theoretical membrane potential derived from Nernst equation. The membrane potential was measured by using a static potential method [2-3]. The test membrane was set in between two cells with an open area of 4.8 cm^2. NaCl solutions of 0.5 M and 0.1 M were filled in the two cells, respectively. Two Ag/ AgCl reference electrodes (Hanna Instruments, USA) were used two measure the potential difference across the membrane. The solutions in the two cells were vigorously stirred by using magnetic stir bars during the process, to minimize diffusion boundary layer effect. The apparent permselectivity was then calculated by:

$$\alpha(\%) = \frac{\Delta V_{measured}}{\Delta V_{theoretical}} \times 100\% \quad \text{(S6)}$$

Membrane ionic resistance was measured by using a four-compartment Plexiglas cell [2]. Totally three membranes were set inside the measuring system, the membrane in the center was the one under investigation, and the other two were commercial FKS (Fumasep®, Fumatech, Germany) CEMs. All membranes were stabilized and had effective area of 7.9 cm^2. All four compartments were filled with 0.5 M of NaCl solution, with two outer compartments having immobile solution, and two inner compartments having inflow and outflow. The water flows were managed by using two peristaltic pumps (Cole-Parmer, USA). Two titanium electrodes covered with platinum were placed at edges of the outer compartments, and were connected to a power supply. Different current densities were applied and corresponding potentials were recorded. The resistance was obtained by the slope of current density versus the potential drop. The final membrane ionic resistance was calculated by subtracting the measured blank resistance (solution resistance) from the measured resistance.

S4. AFM Phase Images of Membrane Surface

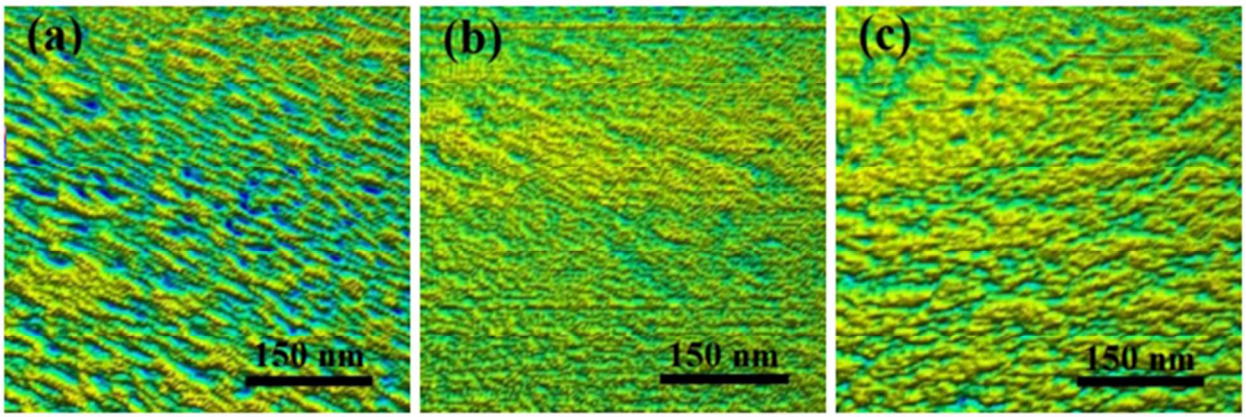

Figure S2. AFM phase images of (a) membrane 1, (b) membrane 3a and (c) membrane 3b.

Tapping mode AFM phase images of membrane surface were obtained, on an area of 500 nm × 500 nm. Since the membrane surface roughness could influence the surface phase [4] , only the regions with low morphological changes were recorded. Fig. S2 shows the phase images of membranes 1, 3a and 3b. The lower domains indicate the soft and hydrophilic ionic clusters, and the higher domains correspond to the hard and hydrophobic polymer backbone. Generally, the hydrophilic ionic clusters are responsible for ion transport, and the hydrophobic domains maintain the stiffness and stability of the membrane [5]. Fig. S2 shows nanophase separation morphology [4, 6], and some of the hydrophilic regions interconnect with each other to some degree. In literature, tapping mode AFM image has been extensively utilized to detect membrane microscale ion channels [5-7], and in many cases the structural difference could be successfully distinguished for membranes with different microscale structures. Moreover, SEM or TEM images were also applied sometimes to characterize membrane microscale structures [8]. In this study, membrane 1 contains more lower domains than membrane 3a and membrane 3b.

The change of the small scale (500 nm × 500 nm) membrane morphology (phase images) might be due to the incorporation of nanomaterials; however, to get more detailed information of the membrane hydrophilic-hydrophobic domain relation and distribution, larger scale (50 μm × 50 μm) AFM phase images were obtained. Larger scale phase images contain more points; thus

they are more statistically significant. Furthermore, instead of categorizing the membrane domains into distinctly hydrophilic or hydrophobic, we classified different parts of membrane area according to the degree of stiffness by using Slice function in Pico Image software. At least six measurements were conducted for each sample. Figure S3 shows the large-scale phase images and stiffness distributions of all the membrane samples. The larger number of degree, which results from larger water swelling on hydration of the material, indicates the more hydrophilic nature of the material. Different degrees of stiffness represent by different colors in the phase images. It is obvious that with the addition of NPs, degree distribution shifts to the right, meaning that the number of relatively hydrophilic domains as well as membrane mean surface hydrophilicity increased.

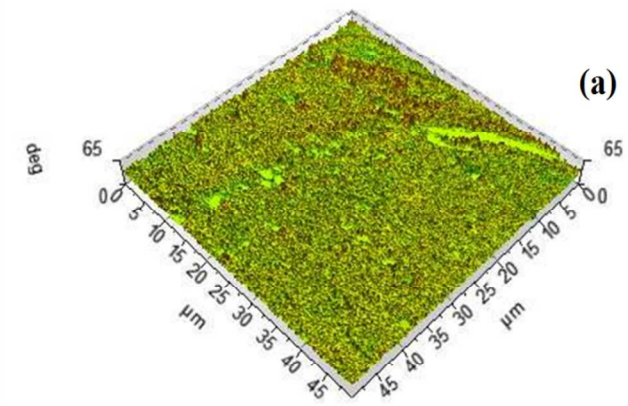
(a)
deg
65
0
μm

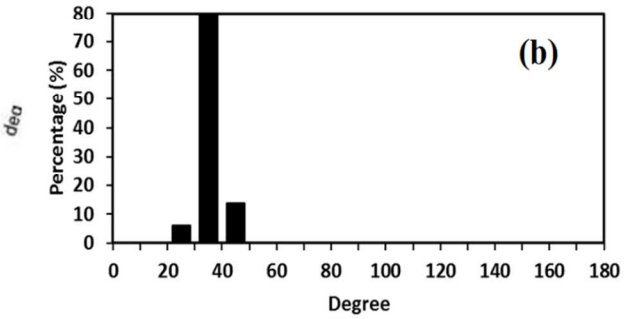
(b)
Percentage (%)
Degree

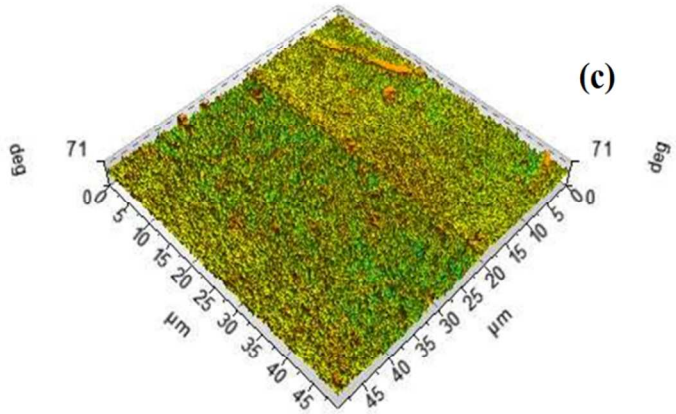
(c)
deg
71
0
μm

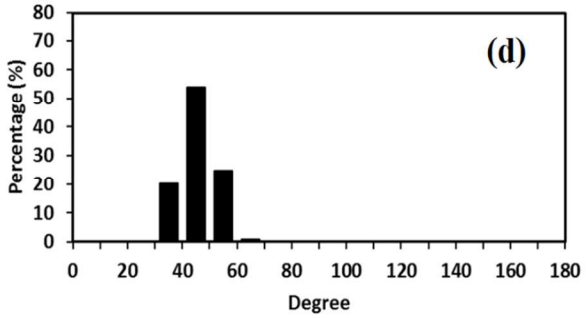
(d)
Percentage (%)
Degree

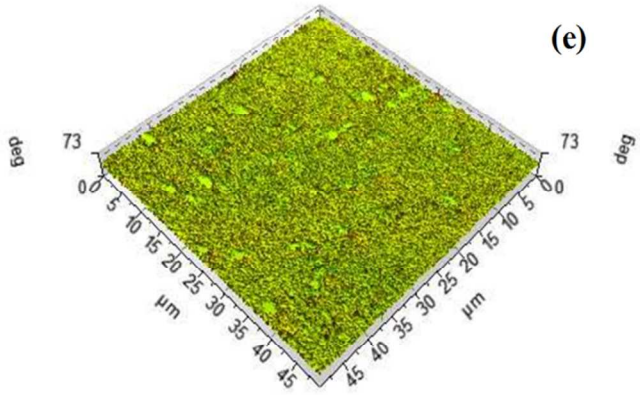
(e)
deg
73
0
μm

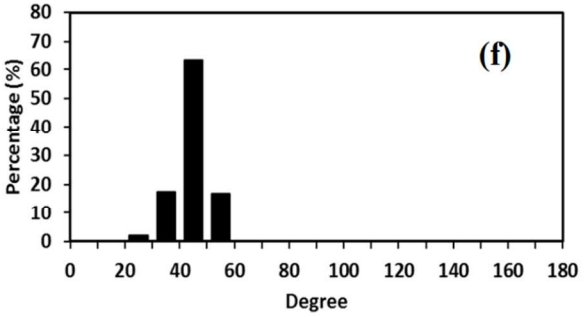
(f)
Percentage (%)
Degree

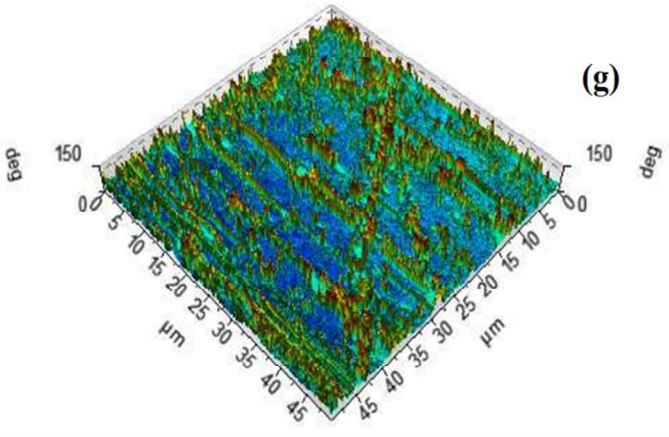
(g)
deg
150
0
μm
0
5
10
15
20
25
30
35
40
45

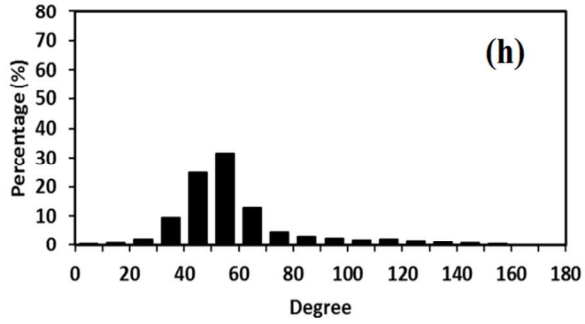
(h)
Percentage (%)
80
70
60
50
40
30
20
10
0
0
20
40
60
80
100
120
140
160
180
Degree

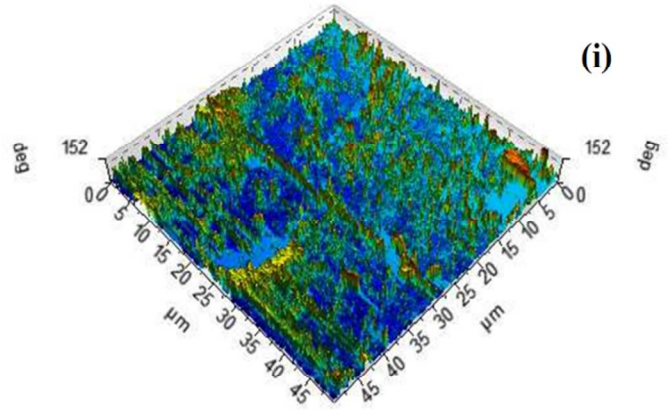
(i)
deg
152
0
μm
0
5
10
15
20
25
30
35
40
45

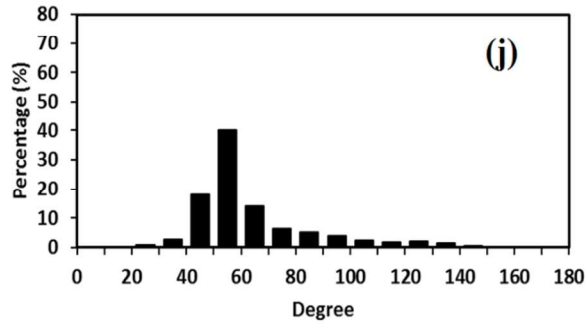
(j)
Percentage (%)
80
70
60
50
40
30
20
10
0
0
20
40
60
80
100
120
140
160
180
Degree

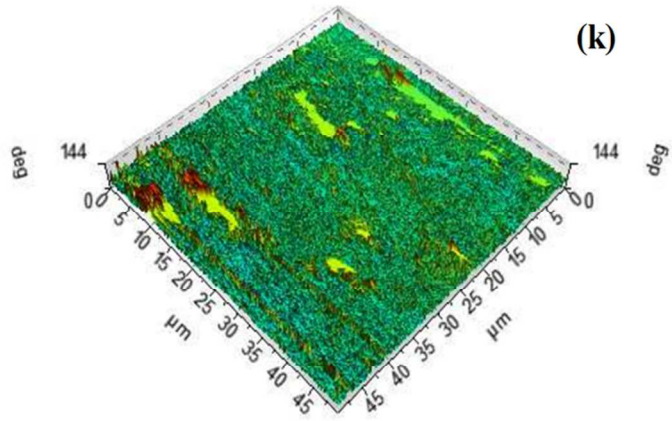
(k)
deg
144
0
μm
0
5
10
15
20
25
30
35
40
45

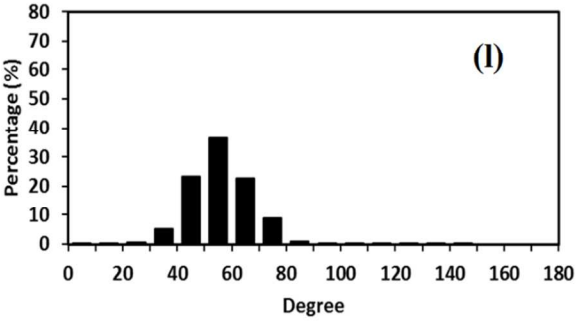
(l)
Percentage (%)
80
70
60
50
40
30
20
10
0
0
20
40
60
80
100
120
140
160
180
Degree

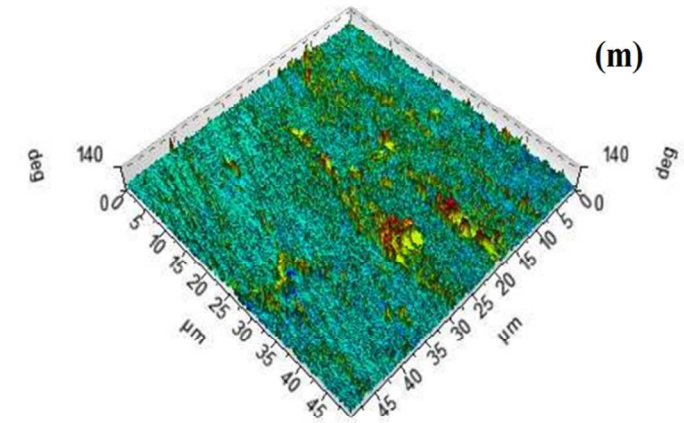
(m)
deg
140
0
0
5
10
15
20
25
30
35
40
45
μm
deg

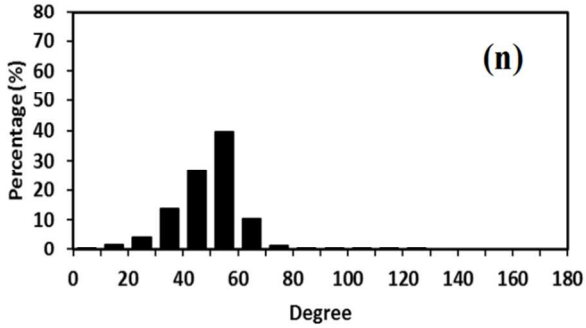
(n)
Percentage (%)
80
70
60
50
40
30
20
10
0
0
20
40
60
80
100
120
140
160
180
Degree

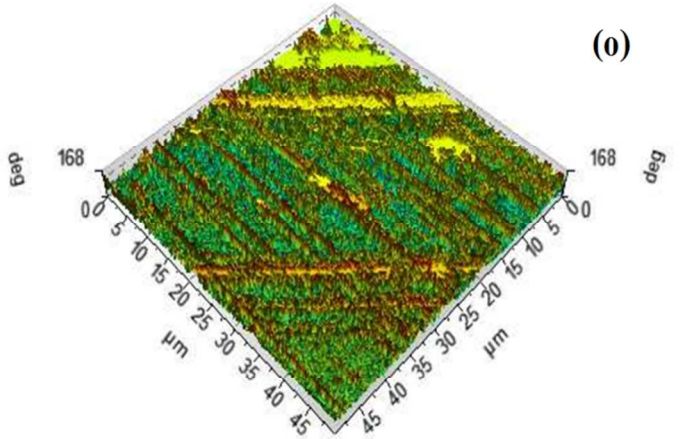
(o)
deg
168
0
0
5
10
15
20
25
30
35
40
45
μm
deg

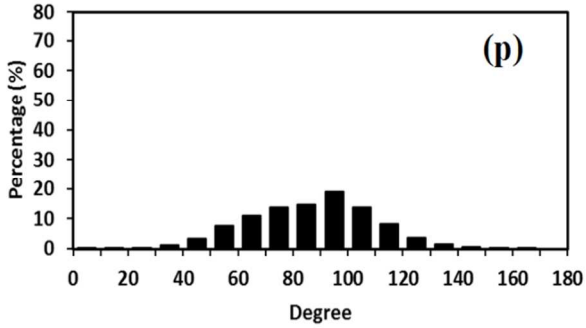
(p)
Percentage (%)
80
70
60
50
40
30
20
10
0
0
20
40
60
80
100
120
140
160
180
Degree

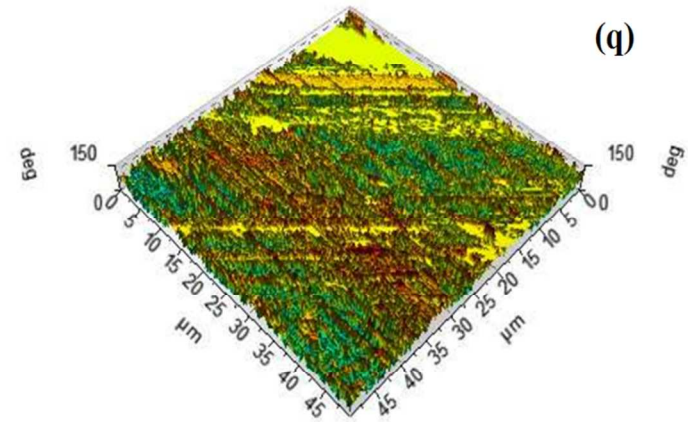
(q)
deg
150
0
0
5
10
15
20
25
30
35
40
45
μm
deg

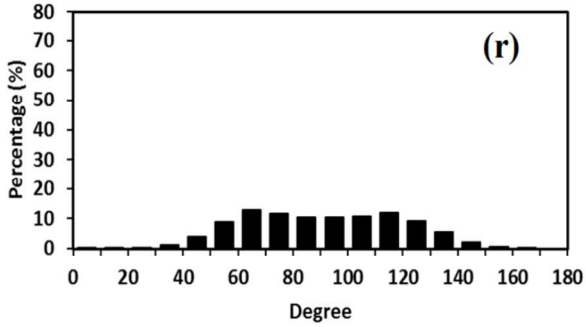
(r)
Percentage (%)
80
70
60
50
40
30
20
10
0
0
20
40
60
80
100
120
140
160
180
Degree

Figure S3. Large scale (50 μm × 50 μm) phase images of (a) membrane 1, (c) membrane 2a, (e) membrane 2b, (g) membrane 3a, (i) membrane 3b, (k) membrane 4a, (m) membrane 4b, (o) membrane 5a, and (q) membrane 5b; areal phase (stiffness) distributions of (b) membrane 1, (d) membrane 2a, (f) membrane 2b, (h) membrane 3a, (j) membrane 3b, (l) membrane 4a, (n) membrane 4b, (p) membrane 5a, and (r) membrane 5b.

S5. Additional SEM Image and EDX Results

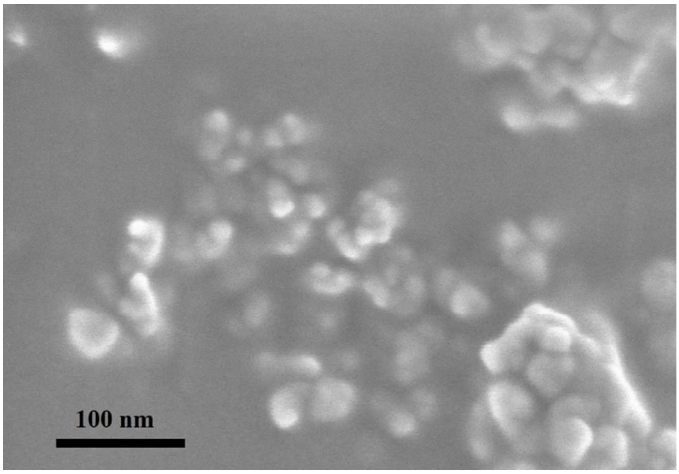

Figure S4. SEM image of silica nanoparticles.

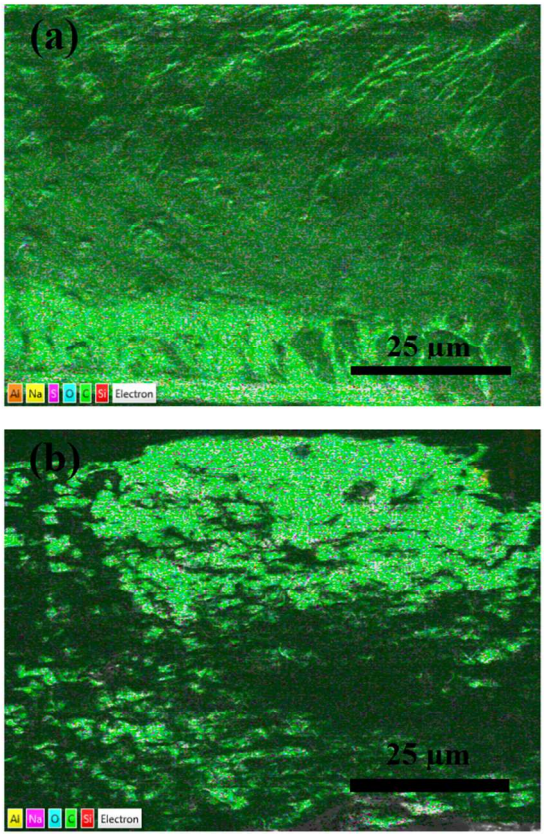

Figure S5. Cross-sectional EDX images of (a) Membrane 5a, and (b) Membrane 5b.

Table S1. Cross-sectional carbon and silicon elements weight percentages of selected membranes by EDX

Membranes	C (wt%)	Si (wt%)
Membrane 3a	73.7	0.1
Membrane 3b	76.7	0.1
Membrane 5a	77.4	0.2
Membrane 5b	76.1	0.3

S6. Membrane Ionic Resistance and Conductivity

Table S2. Measured membrane ionic resistance (R) in different solution concentrations

Membranes	Membrane ionic resistance [Ω cm^2] in different solution concentrations				
	0.01M	0.02M	0.05M	0.08M	0.1M
Membrane 1	16.81±0.56	13.49±0.46	7.92±0.33	5.69±0.18	4.81±0.26
Membrane 2a	16.29±0.35	12.97±0.39	7.19±0.46	5.11±0.25	4.17±0.17
Membrane 2b	16.22±0.29	12.63±0.48	7.48±0.25	5.35±0.27	4.12±0.39
Membrane 3a	16.39±0.75	12.78±0.64	7.27±0.19	5.39±0.19	4.17±0.34
Membrane 3b	16.24±1.16	12.83±0.29	7.37±0.36	5.21±0.46	4.22±0.29
Membrane 4a	15.92±0.09	12.18±0.46	6.77±0.43	4.83±0.43	3.62±0.11
Membrane 4b	16.03±0.26	12.24±0.75	6.94±0.26	4.68±0.27	3.67±0.03
Membrane 5a	16.34±0.46	12.72±0.81	7.35±0.41	5.26±0.61	4.25±0.15
Membrane 5b	16.28±0.49	12.64±0.40	7.38±0.18	5.32±0.24	4.18±0.27

Table S3. Calculated membrane conductivity (k_m) in different solution concentrations

Membranes	Membrane conductivity [μS cm^{-1}] in different solution concentrations				
	0.01M	0.02M	0.05M	0.08M	0.1M
Membrane 1	464.0±15.0	578.2±19.1	984.9±39.4	1370.8±42.0	1621.6±83.2
Membrane 2a	570.9±12.0	717.0±20.9	1293.5±77.8	1819.9±84.9	2230.2±87.4
Membrane 2b	579.5±10.2	744.3±27.2	1256.7±40.6	1757.0±84.4	2281.6±197.3
Membrane 3a	597.9±26.2	766.8±36.6	1348.0±34.3	1818.2±61.9	2350.1±177.2
Membrane 3b	603.5±40.2	763.8±16.9	1329.7±61.9	1881.0±152.6	2322.3±149.3
Membrane 4a	571.6±32.2	747.1±27.2	1344.2±80.3	1884.1±154.0	2513.8±74.1
Membrane 4b	555.2±8.9	727.1±42.0	1282.4±46.3	1901.7±103.7	2425.1±19.7
Membrane 5a	538.6±14.7	691.8±41.4	1197.3±63.3	1673.0±173.9	2070.6±70.6
Membrane 5b	595.8±17.4	767.4±23.5	1314.4±31.3	1823.3±78.7	2320.6±140.8

S7. Degree of Sulfonation and Volume Fraction of Pure Gel Phase

The degree of sulfonation (DS) of polymers could be calculated by:

$$DS = \frac{IEC}{1000 \times [\frac{(1 - M_{SPPO} \times \frac{IEC}{1000})}{M_{PPO}} + \frac{IEC}{1000}]} \times 100\% \text{ (S7)}$$

where M_{SPPO} is the molar weight (g/ mol) of sulfonated PPO, and M_{PPO} is the molar weight (g/ mol) of PPO. Theoretically, all the SPPO in this study should have the same DS, since all the PPO were sulfonated from the same batch. However, it is obvious that the addition of NPs increased the IEC of membranes, thus we rationalized the fact by assuming that the NPs change the DS of membrane polymeric material. So that different membranes could be treated as they were synthesized by using polymer of different DS.

By assuming that all the monomers, whether sulfonated or not, occupy the same volume in the matrices, volume fraction of pure gel phase (f_{11}) could be obtained as the product of DS and polymer gel phase (f_1), and the rest of the gel phase is occupied by inert polymer phase (f_{12}):

$$f_{11} = DS \times f_1 \text{ (S8)}$$

$$f_{12} = f_1 - f_{11} \text{ (S9)}$$

Table S4. Degree of sulfonation and different membrane gel phases

Membranes	f_1 [%]	DS [%]	f_{11} [%]	f_{12} [%]
Membrane 1	44.8	30.9	13.8	31.0
Membrane 2a	40.1	33.7	13.5	26.6
Membrane 2b	41.6	33.7	14.0	27.6
Membrane 3a	41.2	33.4	13.8	27.4
Membrane 3b	41.2	34.0	14.0	27.2
Membrane 4a	36.8	37.4	13.8	23.0
Membrane 4b	36.4	37.0	13.5	22.9
Membrane 5a	41.5	32.2	13.4	28.1
Membrane 5b	41.6	32.5	13.5	28.1

S8. Measured Porosity of Membranes

Membrane porosity was calculated by using the method in S3. Porosity of all the synthesized membranes (wet state) is listed in Table S4. Standard deviations are not included.

Table S5. Porosity of synthesized membranes

Membranes	Porosity [%]
Membrane 1	55.4±3.6
Membrane 2a	57.8±5.7
Membrane 2b	57.0±2.6
Membrane 3a	59.1±4.3
Membrane 3b	58.5±6.2
Membrane 4a	65.7±1.7
Membrane 4b	62.2±4.7
Membrane 5a	55.6±5.9
Membrane 5b	58.8±4.7

S9. Effective Ion Diffusion Coefficient and Tortuosity Factor of Additional CEMs

SPPO based functionalized iron oxide [1] nanocomposite CEMs were discussed. Effective ion diffusion coefficient (presented as D_{eff}/ D) and tortuosity factor (τ) of all the CEMs were calculated by using equations (2) and (3). Membrane porosity data was used as the volume fraction of electrolyte solution phase in membrane, since they have the same physical meaning, and their values were attested to be approximately the same for nanocomposite silica NP CEMs. For iron oxide nanocomposite CEMs, porosity data was taken from the reference [1]. Membrane ionic resistance in 0.5 M of sodium chloride solution was used to calculate the membrane molar conductivity. For iron oxide nanocomposite CEMs, only membranes with thickness of 100 μm and 40 min of evaporation time were included in the discussion. More detailed information about the nanocomposite CEMs could be found in the corresponding references.

Table S6. Porosity of additional nanocomposite CEMs

Membranes	Porosity [%]
0-100 T	47.0
0.3-100 T	52.0
0.7-100 T	56.0

Table S7. Effective diffusion coefficient of additional nanocomposite CEMs

Membranes	D_{eff}/D
0-100 T	0.020
0.3-100 T	0.039
0.7-100 T	0.042

Table S8. Tortuosity factor of additional nanocomposite CEMs

Membranes	τ
0-100 T	23.62
0.3-100 T	13.39
0.7-100 T	13.30

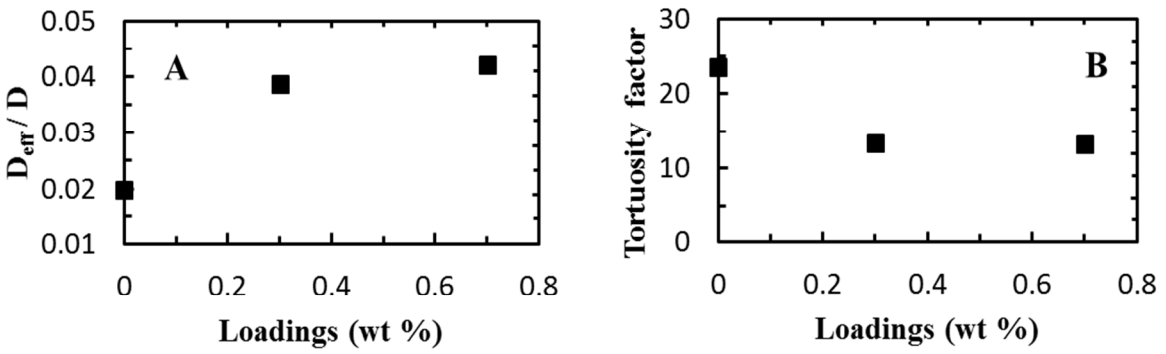

Figure S6. Additional list of diffusion coefficient ratio and tortuosity of discussed CEMs. (A) D_{eff}/ D and (B) Tortuosity factor of CEMs with iron oxide (only membranes with thickness of 100 μm are shown; standard deviations are not included, since they are not shown in the corresponding reference).

S10. Simulation of Nanoparticle Aggregation in Casting Solution

The concentration of nanoparticles added to the casting solution needs to be estimated before compared to the diffusivity. For large spherical nanoparticles, it can be assumed that the volume of the particle (V_p) is the overall volume of basic unit (V_{unit}).

$$V_p = NV_{unit} \quad \text{(S10)}$$

The number of basic unit in a particle is denoted N. If the diameter of nanoparticles (D_p) is deduced from TEM images, then, the estimation of unit diameter (D_{unit}) is possible as we have:

$$D_p = N^{1/3} D_{unit} \quad \text{(S11)}$$

Therefore, the number of units (molecules) N in a nanoparticle is [9]:

$$N = \left(\frac{D_p}{D_{unit}} \right)^3 \quad \text{(S12)}$$

For silica and iron oxide nanoparticles, the mole weight is summarized in Table S9.

Table S9. Data of corresponding nanoparticles

Nanoparticles	Diameter (nm) of single unit	Molar weight (g/ mol) of single unit	Molar weight of single nanoparticles	Reference
SiO_2 (17 nm)	0.342	60	4.05E+7	This study
SiO_2 (30 nm)	0.342	60	7.37E+6	[10]
SiO_2 (420 nm)	0.342	60	1.11E+11	[11]
SiO_2 (30 nm)	0.342	60	7.37E+6	[12]
Fe_2O_3 (30 nm)	0.830	160	7.56E+6	[1]

Model development

Assumedly, the effective diffusivity is determined by the number concentration of nanoparticles incorporated into the polymer structure and the size of the nanocomposite structure:

$$D_{eff} = a + b \cdot \rho_n \quad \text{(S13)}$$

The number concentration of nanomaterial groups, ρ_n, is calculated as the nanomaterial numbers in a given volume; a and b here are fitting constants for linear regression. To obtain the number of nanoparticle groups after the aggregation of individual particles, we also need to know the resulted number of groups given the number of nanoparticles we introduce to the casting solution. The characteristic relationship between the amount of nanoparticle added and the effective diffusivity can be simulated by a statistical model considering the aggregation of nanoparticles in the casting solution matrices.

The model assumes that at the micro-scale, van der Waals force is the dominating form of interactions between nanoparticles [13-14]. The interaction energies between two similar particles can be calculated using van der Waals energy equation from DLVO theory expressed as:

$$V_A = -\frac{A a_1 a_2}{12h(a_1 + a_2)(1 + 11.12h/\lambda_c)} \quad \text{(S14)}$$

where a_1 and a_2 are radius of two nanoparticles, A is the Hamaker constant, nonetheless different from the value used in common aqueous environment. However, the constant is equivalently adjusted as the threshold energy is fit to experimental data as explained in the following; h is the distance between two surfaces of particles, λ_c is the character wavelength (taken as 100 nm generally) [10]. By applying the model, we can get pairwise binding energy of every two particles, assuming only two-body interactions. Because of high viscosity of casting solution, the nanoparticle groups would be stable after formation, especially considering the membrane forming after casting of blend solution on a glass plate surface. Therefore, formed groups will not dissociate into single particles. An energy threshold value has been chosen as a cutoff because the aggregation can only progress within a limited time before solvent evaporation which leads to the drying-out.

Algorithm:

The input of the model is added particle numbers; the output is resulted number concentration of nanomaterial groups and fit to linear model to D_{eff}/D. The program is coded in Matlab 2016b (education edition, MathWorks®). A certain number of particles are initialized randomly with radius and position coordinates in 3-D space. For each pair of particles, the van der Waals energy

is calculated and the inverse of these values are saved as matrix *A*. *A* is then used in the agglomerative hieratical clustering algorithm with a threshold as the implementation of energy cut-off , and 'average' method was used for clustering [15]. The resulted group numbers can be obtained by counting cluster numbers given the threshold.

The added particle values are varied and at each value, 50 replicates are recorded. The results are shown the following figure indicating the simulation in 1 μm^3 space with initial particles ranging from 0 to 2500. Particle diameter is normally distributed with mean of 20 nm and standard deviation of 1 nm. Fitted values is obtained by minimize the root mean square error of averaged simulated values with respect to experimental data. Energy threshold and fitting constants are summarized in Table S10.

Table S10. Parameters of corresponding nanoparticles

Nanoparticles	*a*	*b*	Energy threshold (J)	Reference
Silica NPs (unsolfonated)	0.233	0.0117	2.86E-24	This study
Silica NPs (solfonated)	0.227	0.0134	2.63E-24	This study
Iron oxide (100 μm)	0.200	0.0083	1.00E-23	[1]
Silica NPs (30 μm)	0.451	0.0119	1.12E-23	[10]
Silica NPs (30 μm)	0.579	0.0074	5.05E-23	[12]
Silica NPs (420 μm)	0.550	0.0042	3.61E-24	[11]

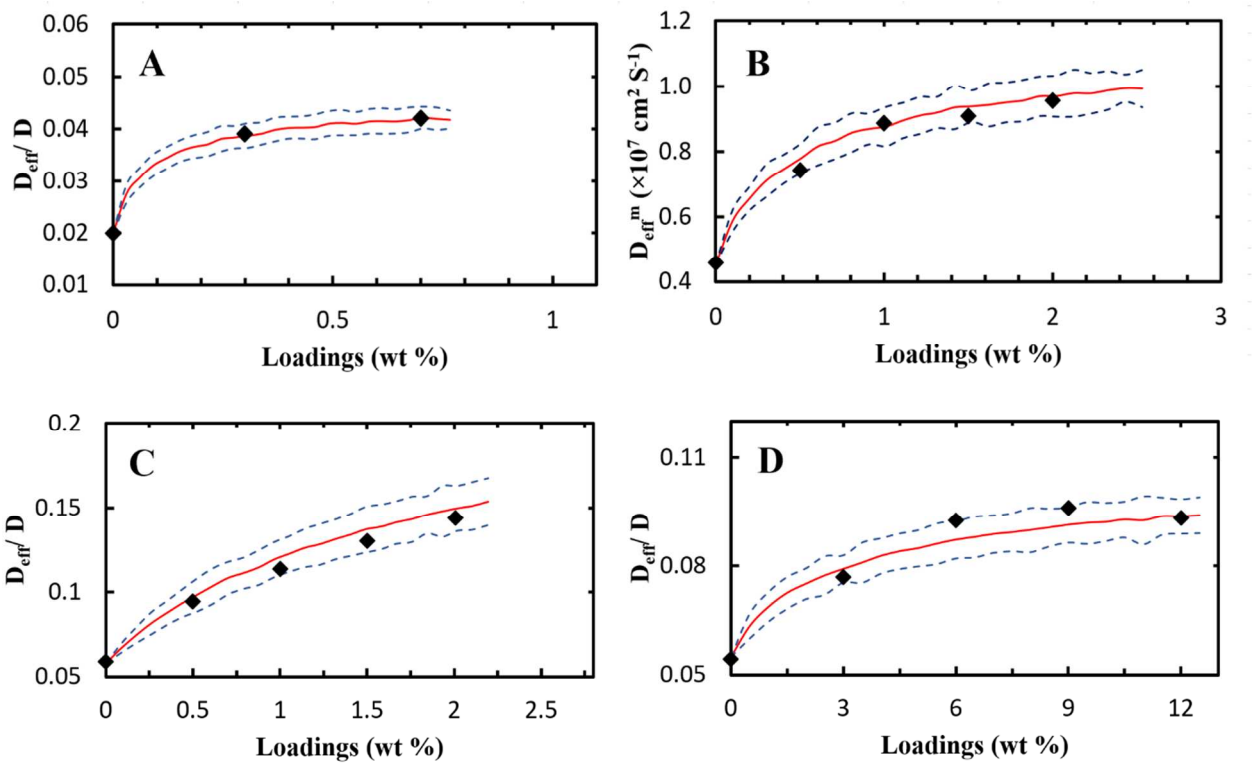

Figure S7. (A) D_{eff}/D of sulfonated iron oxide based, (B) D_{eff}^{m} of silica (30 nm) based (C) D_{eff}/D of silica (30 nm) +based, and (D) D_{eff}/D of silica (420 nm) based nanocomposite IEMs as function of loadings (black dots are the experimental results, red lines are the average values of simulation, and blue dash lines are two standard deviations ($\mu \pm 2\sigma$)).

S11. Matlab Codes of Simulation Model

binding_energy.m

```
function energy = binding_energy(single, whole)

% taking as arguments a 1-by-N vector <single> containing a single
observation
% from points, an M2-by-N matrix <whole> containing multiple observations
from
% points, and returning an M2-by-1 vector of distances D2, whose Jth
% element is the force between the observations single and whole(J,:).

%% The following calculation citing Abu-Lail et al. 2003 and Schenkel et al.
% 1960 in Supporting Information

% Hamaker coefficient
A = 1E-20;
% distance between centers of spheres
dist = pdist2(single(2:end), whole(:, 2:end));

% inter surface distance D = r - R1 - R2
D = dist' - single(1) - whole(:,1);
% avoid the negative value if two points are initilized closer than their
radius combined
D(D<0) = min(D(D>0));
energy = A * single(1)*whole(:,1)./(single(1)+whole(:,1)) ./ D ./ (1 +
11.12*D / 1E-7);

%}

end
```

plot_fitting.m

```
%% Author: Bopeng Zhang; December 30, 2016
% this script takes experimental data and tries to find the best fitting
% of energy threshold

clear variables;
% different weight content of nanoparticles tested in experiments; vary for
% different nanomaterials as inputs
loading = [0, 0.005, 0.01, 0.015, 0.02];
% experimental data of effective diffusivity for different loadings
% vary for different nanomaterials as inputs
data = [0.4578, 0.7438, 0.8878, 0.9091, 0.9565];
% density of membrane in unit g/um^3. We are dealing with 1 um^3 of
% material only
rho_m = 1E-12;
% molar weight of 1 mol of nanoparticles in g/mol
W_n = 4.05E7;
```

```
% calculating number of nanoparticles originally added
Av = 6.02E23; % Avogadro number
np = floor(rho_m / W_n * Av * loading); % number of nanoparticles added
REP = 10; % replicate times of simulation
observed = zeros(length(np),REP);
threshold = 8.85E22; % initialize the inverse of threshold energy
RADIUM = 15e-9; % particle redius

old_SS = 10;
SSresid = 100;
i = 1;
step = 1;
while abs(old_SS-SSresid) > 1E-9
    old_SS = SSresid;
    for j = 1:REP
        i = 1;
        for number = np
            if number == 0
                observed(i, j) = 0;
            else
                % first data store radius of particle
                radius = normrnd(RADIUM, 1E-9, [number, 1]);
                radius(radius<0) = RADIUM;
                % random initialization in 1 um^3
                points = [radius 1E-6*rand([number,3])];
                % follow the clustering algorithm
                energy_distance = 1./pdist(points,@binding_energy);

                Z = linkage(energy_distance, 'average');
                T = cluster(Z, 'cutoff', threshold, 'criterion','distance');
                % resulted group number is the groups number of clusters
                observed(i, j) = max(T);
            end
            i = i + 1;
        end

    end
    sim = mean(observed, 2);

    % fit a linear regression model and calculate sum of squared residuals
    p = polyfit(sim', data, 1);
    yfit = polyval(p, sim');
    yresid = data - yfit;
    SSresid = sum(yresid.^2);
    fprintf('This is run %d at the cut-off of %.2e; the SSresid is %.6f.\n',
step, 1/threshold, SSresid);
    threshold = threshold + 1E21;
    step = step + 1;

end

plot(np, data);hold on; plot(np, yfit)
```

plot_fitting_line.m

```
%% Author: Bopeng Zhang; December 30, 2016
% this script takes the best energy threshold and generates the simulated
% diffusivity (or effective diffusivity)

clear variables;
% simulation on 25 points on x-axis
list = 1:25;
observed = zeros(50,length(list));
% fitting parameters a and b for linear regression; get from fitting.m
a = 0.451; b = 0.0124;
% replicate for 50 times
for j = 1:50
    for i = list
        NUMBER = i*15; THRESHOLD = 8.93E22; RADIUM = 15E-9;

        % first data store radius of particle; three coordinates later
        radius = normrnd(RADIUM, 1E-9, [NUMBER, 1]);
        radius(radius<0) = RADIUM;
        % random initialization in 1 um^3
        points = [radius 1E-6*rand([NUMBER,3])];

        energy_distance = 1./pdist(points,@binding_energy);

        Z = linkage(energy_distance, 'average');
        T = cluster(Z, 'cutoff', THRESHOLD, 'criterion','distance');
        observed(j,i) = max(T);
    end
    plot(list*15, a+b*observed(j,:),'.');
    hold on;
    display(j);
end

xlabel('Added particle number');
ylabel('Effective diffusivity/diffusivity');
```

Reference

(1) Hong, J. G.; Chen, Y., Evaluation of Electrochemical Properties and Reverse Electrodialysis Performance for Porous Cation Exchange Membranes with Sulfate-Functionalized Iron Oxide. *J. Membr. Sci.* **2015,** *473*, 210-217.
(2) Hong, J. G.; Chen, Y., Nanocomposite Reverse Electrodialysis (RED) Ion-Exchange Membranes for Salinity Gradient Power Generation. *J. Membr. Sci.* **2014,** *460*, 139-147.
(3) Tong, X.; Zhang, B.; Chen, Y., Fouling Resistant Nanocomposite Cation Exchange Membrane with Enhanced Power Generation for Reverse Electrodialysis. *J. Membr. Sci.* **2016,** *516*, 162-171.
(4) Amel, A.; Gavish, N.; Zhu, L.; Dekel, D. R.; Hickner, M. A.; Ein-Eli, Y., Bicarbonate and Chloride Anion Transport in Anion Exchange Membranes. *J. Membr. Sci.* **2016,** *514*, 125-134.
(5) Tan, N.; Xiao, G.; Yan, D., Sulfonated Polybenzothiazoles: A Novel Candidate for Proton Exchange Membranes†. *Chem. Mater.* **2009,** *22*, 1022-1031.
(6) McLean, R. S.; Sauer, B. B., Tapping-Mode AFM Studies Using Phase Detection for Resolution of Nanophases in Segmented Polyurethanes and Other Block Copolymers. *Macromolecules* **1997,** *30*, 8314-8317.
(7) Leclère, P.; Lazzaroni, R.; Brédas, J.-L.; Yu, J. M.; Dubois, P.; Jérôme, R., Microdomain Morphology Analysis of Block Copolymers by Atomic Force Microscopy with Phase Detection Imaging. *Langmuir* **1996,** *12*, 4317-4320.
(8) Diat, O.; Gebel, G., Fuel Cells: Proton Channels. *Nat. Mater.* **2008,** *7* (1), 13-14.
(9) Lewis, D. J.; Day, T. M.; MacPherson, J. V.; Pikramenou, Z., Luminescent Nanobeads: Attachment of Surface Reactive Eu (III) Complexes to Gold Nanoparticles. *Chem. Commun.* **2006,** 13, 1433-1435.
(10) Zuo, X.; Yu, S.; Xu, X.; Xu, J.; Bao, R.; Yan, X., New PVDF Organic–Inorganic Membranes: the Effect of SiO2 Nanoparticles Content on the Transport Performance of Anion-Exchange Membranes. *J. Membr. Sci.* **2009,** *340*, 206-213.
(11) Kim, J.-H.; Kim, S.-K.; Nam, K.; Kim, D.-W., Composite Proton Conducting Membranes Based on Nafion and Sulfonated SiO2 Nanoparticles. *J. Membr. Sci.* **2012,** *415*, 696-701.
(12) Zuo, X.; Yu, S.; Xu, X.; Bao, R.; Xu, J.; Qu, W., Preparation of Organic–Inorganic Hybrid Cation-Exchange Membranes via Blending Method and Their Electrochemical Characterization. *J. Membr. Sci.* **2009,** *328*, 23-30.
(13) Abu-Lail, N. I.; Camesano, T. A., Role of Ionic Strength on the Relationship of Biopolymer Conformation, DLVO Contributions, and Steric Interactions to Bioadhesion of P seudomonas p utida KT2442. *Biomacromolecules* **2003,** *4*, 1000-1012.
(14) Schenkel, J.; Kitchener, J., A Test of the Derjaguin-Verwey-Overbeek Theory with a Colloidal Suspension. *Trans. Faraday Soc.* **1960,** *56*, 161-173.
(15) Agglomerative Hierarchical Cluster Tree - MATLAB Linkage. https://www.mathworks.com/help/stats/linkage.html?requestedDomain=www.mathworks.com;%20https://www.mathworks.com/help/stats/cluster.html&requestedDomain=www.mathworks.com (accessed Feb 20, 2017).